An Analysis of Actin Delivery in the Acrosomal Process of *Thyone*

Donald J. Olbris and Judith Herzfeld
Dept. of Chemistry and Keck Institute for Cellular Visualization, Brandeis University, Waltham, Massachusetts 02454-9110 USA

ABSTRACT The acrosomal process of the sea cucumber *Thyone briareus* can extend 90 μm in 10 s, but an epithelial goldfish keratocyte can only glide a few microns in the same time. Both speeds reflect the rate of extension of an actin network. The difference is in the delivery of actin monomers to the polymerization region. Diffusion supplies monomers fast enough to support the observed speed of goldfish keratocytes, but previous models have indicated that the acrosomal process of *Thyone* extends too rapidly for diffusion to keep up. Here we reexamine the assumptions made in earlier models and present a new model, the Actin Reconcentration Model, that includes more biological detail. Salt and water fluxes during the acrosomal reaction and the nonideality of the cytoplasm are particularly significant for actin delivery. We find that the variability of the acrosomal growth curve can be explained by the salt and water fluxes, and that nonideality magnifies the effect of actin concentration changes. We calculate the speed of process growth using biologically relevant parameters from the literature and find that the predictions of the model fall among the experimental data.

INTRODUCTION

Humans and other vertebrates do not grow new limbs to walk or reach. They simply move the limbs they already have using the attached muscles. Cells employ different tactics. By controlled, localized polymerization of actin monomers, cells create a variety of protrusions and extensions with which to crawl, reach, and glide. Cytoskeletal rearrangement is used for cell locomotion (Bray and White, 1988; Cooper, 1991; Mitchison and Cramer, 1996) and cell protrusion (Condeelis, 1993; Oster and Perelson, 1987), including fibroblast migration (Conrad et al., 1989; DeBiasio, et al., 1988), neuronal growth cone extension (Smith, 1988), and amoeba motility (Grebecki, 1994). Some pathogens also use their host's actin to move. *Listeria monocytogenes* (Cossart, 1995; Southwick and Purich, 1994; Tilney et al., 1992a, b), *Shigella flexneri* (Goldberg and Theriot, 1995; Theriot, 1995), members of the *Rickettsia* family (Heinzen et al., 1993; Teysseire et al., 1992), and the Vaccinia virus (Cudmore et al., 1995) initiate polymerization of actin into "comet tails" that propel them through the cytoplasm. Another pathogen, enteropathogenic *Escherichia coli*, is propelled over the external surface of a cell by "pedestals" of actin that it induces to form inside the cell (Sanger et al., 1996).

Along with the wide structural variation in systems with actin-based motility, there is a wide range of observed speeds (Condeelis, 1993). Although epithelial goldfish keratocytes and *Listeria* move at speeds of tenths of microns per second (Lee et al., 1993; Theriot and Mitchison, 1991; Theriot et al., 1992), fibroblasts crawl relatively slowly, at <0.01 μm/s (Theriot and Mitchison, 1992). In contrast, the extension of the acrosomal process of the sea cucumber *Thyone briareus* is rapid. When *Thyone* sperm contacts egg jelly, it constructs a thin extension with an actin core: the acrosomal process (Dan, 1967; Inoué and Tilney, 1982). The process grows rapidly and reaches lengths of 60–90 μm in under 10 s (Colwin and Colwin, 1955). By comparison, a fast-moving goldfish keratocyte might take a few minutes to crawl the same distance; a 3T3 fibroblast would take hours (Theriot and Mitchison, 1992).

Like crawling cells, the acrosomal process polymerizes actin into filaments at its leading edge (Tilney, 1978; Tilney and Kallenbach, 1979). It therefore requires the continuous delivery of actin monomers to its tip in order to continue extending. The simplest delivery mechanism is diffusion. As polymerization consumes actin, a concentration gradient forms between the interior reservoir and the leading edge, causing actin monomers to diffuse down the gradient. For crawling goldfish keratocytes, monomers depolymerize at the rear of the lamellipodium and diffuse forward to the leading edge; where they are rendered polymerization-competent. In this system, the diffusive flux is adequate to support the observed motility rate (Olbris and Herzfeld, 1996).

Two features of the acrosomal process make diffusive actin delivery less efficient than in the fish keratocyte. First, because *Thyone*'s acrosomal process reaches such extreme lengths (up to 90 μm compared to the 3–5-μm lamellipodium of a goldfish keratocyte), actin must be transported over much longer distances than in other systems. Diffusive flux decreases inversely with increasing distance. Second, the density of actin filaments in the acrosomal process is far greater than in the fish keratocyte lamellipodium. Not only does the higher density of filaments require an increased flux of actin monomers to maintain the extension speed, but the space occupied by the filaments themselves also reduces the fluid volume available for actin transport.

In any case, to properly explain the process's extension speed, it is necessary to examine more closely what happens during the whole acrosomal reaction, of which the extension

Received for publication 13 May 1999 and in final form 30 August 1999.
Address reprint requests to Dr. Judith Herzfeld, Dept. of Chemistry, MS 015, Brandeis University, 415 South St., Waltham, MA 02454-9110. Tel.: 781-736-2538; Fax: 781-736-2516; E-mail: herzfeld@brandeis.edu.

0006-3495/99/12/3407/17 $2.00

of the acrosomal process is only one step (Colwin and Colwin, 1955; Dan, 1967; Inoué and Tilney, 1982; Tilney and Inoué, 1982). Fig. 1, adapted from Figs. 1 and 6 of Inoué and Tilney (1982), shows a schematic of the three stages in the reaction. In the untriggered sperm (Fig. 1 *a*), actin is located in the periacrosomal region (P), behind the acrosomal vacuole (V). The actin is bound in an insoluble complex with profilin and two high molecular weight proteins (Tilney, 1979; Tilney and Inoué, 1985).

In nature, the acrosomal reaction is triggered by contact with *Thyone* egg jelly, but it can also be triggered in the laboratory with ionophores (Inoué and Tilney, 1982). Several events take place when the reaction is triggered. Movement of Ca^{2+} into the sperm induces the fusion of the front membrane of the acrosomal vacuole (V) and the front membrane of the sperm (Tilney, 1979; Fig. 1, *a* and *b*). The fused membrane subsequently opens, releasing the contents of the vacuole (Inoué and Tilney, 1982). At this point, the rear membrane of the vacuole becomes the front membrane of the acrosomal process.

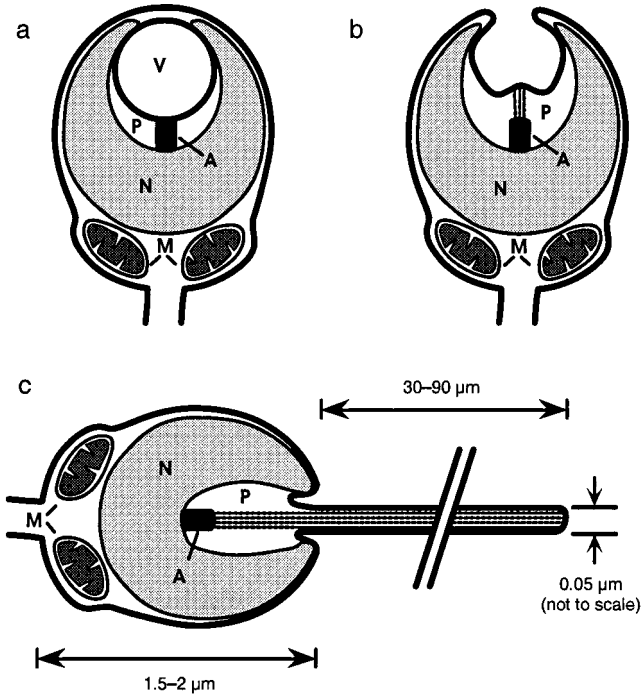

FIGURE 1 A schematic of *Thyone* sperm and its acrosomal process (based on Fig. 1 and Fig. 6 of Inoué and Tilney, 1982). Panel (*a*) shows the intact sperm. The periacrosomal region (P) holds the unpolymerized actin in an inert form between the acrosomal vacuole (V) and the nuclear material (N). The mitochondria (M) are located near the tail of the sperm, which is only partially pictured. In panel (*b*), the acrosomal reaction has been triggered, and the acrosomal process has started to grow. The front membrane of the acrosomal vacuole (V) and the front membrane of the sperm (Tilney, 1979) have fused, and the contents of the vacuole (Inoué and Tilney, 1982) have been released. The rear membrane of the vacuole has become the front membrane of the acrosomal process. Actin polymerization has been nucleated on the actomere (A). The filaments are oriented with their barbed ends pointing away from the body of the sperm. Monomers diffuse from the periacrosomal region to the tip of the process, where they are added to the filaments. In (*c*), the acrosomal process has reached its final length, between 30 and 90 μm. The process, shown with greatly exaggerated thickness, is ~50 nm in diameter and contains ~60 filaments in cross-section. The final shape and size of the periacrosomal region are not known.

Then something striking takes place: the periacrosomal region doubles in volume (Inoué and Tilney, 1982). The doubling occurs rapidly, in 50–70 ms, indicating not only that there is a strong driving force for water to enter the periacrosomal region, but also that the surrounding membrane is quite permeable to water. The water movement is presumably driven by an osmotic pressure change. Although actin is released into solution in the periacrosomal region after the acrosomal reaction is triggered (Tilney et al., 1978), its concentration is not high enough to cause doubling of the compartment's volume, even taking into account the effects of nonideality. Salt, however, is present in much higher concentrations. In another echinoderm, the sea urchin, the acrosomal reaction is accompanied by a 30 mV membrane depolarization that is caused by the influx of ions into the acrosome (Schackmann et al., 1981). Ions also flood the acrosome of *Thyone*, and although the membrane potential has not been measured, it is probably this influx that leads to the observed water influx and volume doubling.

Once actin unbinds from the high molecular weight proteins, polymerization begins. The profilin-actin complex polymerizes onto the actomere (A in Fig. 1), a nucleating organelle (Tilney, 1978), and the profilin is released into solution. The extension of the process then proceeds rapidly (Fig. 1 *c*). Decoration with myosin subfragments reveals that these actin filaments are uniformly oriented with their barbed (fast-growing) ends away from the actomere (Tilney and Kallenbach, 1979). The profilin-actin complex presumably diffuses to the tip of the process where the actin is added to the process. Because nucleotide exchange occurs far more rapidly on profilin-actin than on actin alone (Theriot and Mitchison, 1993), the monomers are expected to be polymerization-competent on arrival at the tip. Processes triggered by ionophores in the laboratory have reached lengths of 30–90 μm in only 5–10 s (Tilney and Inoué, 1982), with growth ceasing rather suddenly.

Several groups have calculated the extension speed of the acrosomal process assuming that actin is delivered by diffusion alone. A model of Tilney and Kallenbach (1979), based on the work of Hermans (1947) and corrected by Perelson and Coutsias (1986), assumes that diffusion delivers actin monomers to the growing filament tips where infinitely fast polymerization takes place. A second model due to Perelson and Coutsias (1986) assumes a finite polymerization rate and includes effects due to fluid movement into the process. Because both models predicted growth rates significantly less than those observed experimentally, it was then believed that diffusion alone could not deliver actin rapidly enough to explain the growth of the process.

The diffusion models noted above are oversimplified. First, neither model takes into account that actin filaments occupy space that could otherwise be used to transport actin. Including the volume of the actin filaments will reduce the

diffusive flux and the extension speed. Second, both models ignore the volume change in the acrosome at the onset of the acrosomal reaction. Because the periacrosomal region doubles in volume before the process begins to extend, the initial actin concentration immediately drops by half, dramatically reducing the diffusive flux to the tip of the process. Third, both models ignore the depletion of actin in the reservoir as the process grows. This depletion will further reduce the diffusive flux of actin.

In the next section we introduce a diffusion-only model for the extension of the acrosomal process that corrects these flaws of previous models. Of course, this corrected diffusion-only model reproduces the experimental data even less well than the earlier models. In the Actin Reconcentration Model we extend the corrected model to include active ion transport, which leads to higher actin concentration, increased diffusive flux, and faster extension speed. In the Actin Reconcentration Model, we also take account of the extreme nonideality due to high protein concentrations in the cell. Using parameter values from the literature, this model predicts behavior within the range of the experimental data.

In the fourth section, we present more detailed versions of the models in the second and third sections. Many of the approximations made in the initial calculations are relaxed, and the resulting equations are solved iteratively. The results of the more detailed models are shown to be in excellent agreement with the initial calculations, thereby justifying the approximations made earlier. In the final sections, we discuss implications and interpretations of the models, and we summarize our conclusions.

DIFFUSION-ONLY MODELS

Minimal models

The system consists of a cylindrical process of radius r and the periacrosomal region, which acts as a "reservoir" of actin and solvent for the growing process. The reservoir's initial volume is known from experimental observations. Actin monomers diffuse from the reservoir to the tip of the process, where they polymerize onto the ends of the filaments. If the concentration of monomers in the reservoir is assumed to be constant, and chemical steps involved in polymerization are infinitely fast, the growth of the acrosomal process can be mapped onto a previously solved diffusion problem (Hermans, 1947). The length of the acrosomal process as a function of time is then given by Tilney and Kallenbach (1979)

$$L(t) = z\sqrt{4D_a t}, \tag{1}$$

where D_a is the diffusion coefficient of the actin monomer. The constant z is given by the solution to

$$z\exp(z^2)\mathrm{erf}(z) = \frac{c_{a,res}}{\sqrt{\pi}}\frac{\delta}{n}, \tag{2}$$

where $c_{a,res}$ is the concentration of actin monomers in the reservoir, δ is the average increase in filament length per monomer added, n is the number of growing filaments per unit cross-sectional area, and $\mathrm{erf}(x)$ is the error function (Arfken, 1985). The concentration of actin monomers in the process, at a distance x from the reservoir, is given by

$$c_a(x,t) = c_{a,res}\left[1 - \frac{\mathrm{erf}(x/\sqrt{4D_a t})}{\mathrm{erf}(L/\sqrt{4D_a t})}\right] \tag{3}$$

for $x < L(t)$.

Perelson and Coutsias (1986) later improved this model by relaxing the assumption of infinitely fast polymerization and including the effects of the movement of fluid into the extending process. Their more complicated singular perturbation analysis gave the same $L \sim \sqrt{t}$ form as before, but their numerical prefactor was smaller.

The forgoing models are difficult to extend because any improvements would probably render them analytically unsolvable. We will formulate a model that is simpler mathematically but gives similar results. This model will then be modified in later sections to include some of the features of the physical system that the previous models ignored.

Inasmuch as it is clear that actin delivery, not actin polymerization, is the limiting factor for growth in this system, we continue to assume that polymerization is infinitely fast. Any actin monomer that diffuses to the end of the process is assumed to be immediately polymerized. The flux of monomers added to the filaments is thus set equal to the diffusive flux of monomers to the tip: $j_{poly} = j_{diff}(L)$.

The diffusive flux is given by Fick's law: $j_{diff} = -D_a\partial c_a/\partial x$. In this system, the actin concentration profile $c_a(x)$ equilibrates quickly. We therefore assume that the actin monomer concentration always reaches the linear profile between the reservoir and tip that it would have in a steady-state, constant length system. The concentration of actin at the tip $c_{a,tip}$ is set to zero due to the assumption of infinitely fast polymerization, so the concentration profile is $c_a(x) = c_{a,res}(1 - x/L)$. That this profile is reasonable can be seen by examining Eq. 3. The error function $\mathrm{erf}(x)$ is fairly linear for $x < 1$. Replacing $\mathrm{erf}(x)$ by a linear function in Eq. 3 gives a linear concentration profile. The diffusive flux is then

$$j_{diff} = -D_a\frac{\partial c_a}{\partial x} = \frac{D_a c_{a,res}}{L}. \tag{4}$$

The flux of monomers j_{poly} being polymerized is directly related to the extension speed v_{ext} by

$$v_{ext} = (\delta/n)j_{poly}. \tag{5}$$

Since $v_{ext} = dL/dt$ and $j_{diff} = j_{poly}$, Eq. 5 becomes a first-order differential equation:

$$\frac{dL}{dt} = \left(\frac{\delta}{n}\right)j_{diff} = \left(\frac{\delta}{n}\right)\frac{D_a}{L}c_{a,res}. \tag{6}$$

With the initial condition $L(0) = L_0$, Eq. 6 can be integrated to

$$L(t) = \sqrt{\frac{2\,D_a c_{a,res}\delta}{n}t + L_0^2}. \quad (7)$$

Equation 7 is much simpler in form and derivation than Eqs. 1 and 2. However, as will be shown in our results, the predictions are nearly identical.

Corrected model

From this starting point we may now correct some flaws in the minimal models. One significant omission in the minimal models is that the volume occupied by the actin filaments is ignored. Actin filaments are densely packed in the acrosomal process, and the available volume through which monomers diffuse to reach the filament tips is reduced. We replace the number of growing filament ends per area n with the number of filament ends per *fluid-accessible* area N_f/A_d, where N_f is the total number of filaments in the process ($N_f = n\pi r^2$), and A_d is the cross-sectional area of the process that is available for diffusion (i.e., not occupied by filaments).

The other changes are in the treatment of the reservoir. First, the reservoir volume swells to approximately twice its initial volume: $V_0 \rightarrow 2V_0$. Second, the concentration of actin monomers in the reservoir is not constant. Initially, $c_{a,res}(0) = N_{a0}/2V_0$, where N_{a0} is the initial number of actin monomers in the reservoir. The number of monomers in the reservoir then drops by the number of monomers that have left. If the relatively few free monomers in the process are ignored, the actin concentration in the reservoir is decreased by the number of monomers that have been added to the actin filaments:

$$c_{a,res}(t) = \frac{N_{a0} - N_f(L/\delta)}{2V_0} = c_{a,res}(0)(1 - L/L_\infty), \quad (8)$$

where $L_\infty = N_{a0}\delta/N_f$ is the length the process would attain when all the monomers in the reservoir are polymerized.

When all of the above corrections are collected, Eq. 6 becomes

$$\frac{dL}{dt} = \delta\left(\frac{A_d}{N_f}\right)\frac{D_a}{L}\frac{N_{a0} - N_f(L/\delta)}{2V_0} = \frac{D_a A_d}{2V_0}\frac{(1 - L/L_\infty)}{L/L_\infty}. \quad (9)$$

This differential equation can be integrated with the initial condition $L(0) = L_0$ to give

$$\frac{L_0 - L}{L_\infty} - \ln\left(\frac{1 - L/L_\infty}{1 - L_0/L_\infty}\right) = \left(\frac{D_a A_d}{2V_0 L_\infty}\right)t, \quad (10a)$$

which cannot be solved for $L(t)$ explicitly. Because $L < L_\infty$, we may use the expansion $\ln(1 - x) = -\sum_{m=1}^{\infty} x^m/m$, to find the following expression for $t(L)$:

$$t(L) = \left(\frac{2V_0 L_\infty}{D_a A_d}\right)\sum_{m=2}^{\infty}\frac{1}{m}\left[\left(\frac{L}{L_\infty}\right)^m - \left(\frac{L_0}{L_\infty}\right)^m\right]. \quad (10b)$$

If only the first term of the series is retained, the $t \sim L^2$ form is recovered (compare Eq. 7). In any case, Eq. 10a can be solved numerically for $L(t)$ by software packages such as *Mathematica* (Wolfram, 1996).

Choice of parameter values

Table 1 summarizes the values of the various parameters used in calculating extension speeds under the diffusion-only models. In reality, the diffusing solute is not actin, but the actin-profilin complex. Its diffusion coefficient D_a is not known. Estimates for the diffusion coefficient of actin vary from 5 to 8×10^{-7} cm^2/s in aqueous solution (Lanni et al., 1981; Lanni and Ware, 1984; Tait and Frieden, 1982). Noting that human hemoglobin, whose molecular weight is ~10% greater than that of profilin and actin together, has a diffusion coefficient of $\sim 5 \times 10^{-7}$ cm^2/s in aqueous solution (Gros, 1978; Muramatsu and Minton, 1988), we take $D_a = 5 \times 10^{-7}$ cm^2/s.

Actin filaments are double-stranded, so the average extension per monomer added is about half the monomer length: $\delta = 2.7$ nm (DeRosier and Tilney, 1984). Electron micrographs show $\sim N_f = 60$ filaments in the cross section of a *Thyone* process with $r = 0.025$ μm (Tilney and Inoué, 1982), so the density of growing ends is $n = N_f/\pi r^2 = 3.1 \times 10^{12}$/cm^2. Some of the cross-sectional area of the process is occupied by the polymerized actin and is not accessible to fluid. Taking the density of protein to be 1.4 g/cm^3 (Cantor and Schimmel, 1980), an actin monomer of 42 kDa then has a volume of $\sim 5.0 \times 10^{-20}$ cm^3. Therefore, the $N_f = 60$ polymerized monomers in a $\delta = 2.7$ nm length of the process occupy $\sim 3.0 \times 10^{-18}$ cm^3, or $\sim 1.1 \times 10^{-11}$ cm^2 of cross-sectional area, leaving $A_d = 8.5 \times 10^{-12}$ cm^2 of the total $\pi r^2 = 2.0 \times 10^{-11}$ cm^2 accessible for diffusion. This corresponds to an average diameter of the actin double strands that is smaller than the maximum diameter reported from atomic models because we are concerned with the volume occupied by the filament rather than the distance between adjacent filaments.

The periacrosomal region, which holds the actin before the process starts to elongate, is estimated to have an initial, pre-doubling volume of $V_0 = 5.1 \times 10^{-13}$ cm^3 (Tilney and Inoué, 1982). Within this volume, actin (42 kDa) is stored in

TABLE 1 Parameter values for the diffusion-only models

Symbol	Parameter	Value
D_a	Actin diffusion coefficient	5.0×10^{-7} cm^2/s
δ	Length increment per actin monomer polymerized	2.7 nm
N_f	Number of actin filaments	60
r	*Thyone* process radius	0.025 μm
A_d	Cross-sectional area accessible for diffusion	8.5×10^{-12} cm^2
V_0	Initial reservoir volume	5.1×10^{-13} cm^3
N_{a0}	Initial number of actin monomers in the reservoir	3.1×10^6
L_0	Initial length of the process	0.19 μm

an insoluble form, along with profilin (16 kDa) and two higher molecular weight proteins (220 and 250 kDa) in a 1:1:1/12:1/12 ratio (Tilney and Inoué, 1982). If 70% of V_0 (midway between face-centered and body-centered close packing) is occupied by those proteins in the given ratio, with an average density of 1.4 g/cm^3, then the reservoir initially contains $\sim N_{a0} = 3.1 \times 10^6$ monomers of actin. That is in excess of the 2×10^6 monomers required to build a 60-filament, 90-μm-long process. After the volume of the periacrosomal region doubles at the onset of the acrosomal reaction, the actin concentration in the reservoir will be $N_{a0}/2V_0$, or $\sim c_{a,res}(0) = 5$ mM. If the swelling is ignored, the concentration is twice as large, 10 mM.

The initial length of the process L_0 is set to 0.19 μm. That particular number is unimportant for this model, but it is chosen for convenience in later comparisons with other models.

Results

We now compare the predictions of the above models to experimental data. Unless otherwise noted, the results for the models were calculated using the parameters in Table 1.

Fig. 2 shows the length of the acrosomal process (μm) plotted as a function of time (s) for the experimental data and the models. The experimental data are taken from Fig. 2 of Tilney and Inoué (1982). Curve (b) is the prediction of the earlier model (Eqs. 1 and 2) (Hermans, 1947; Tilney and Kallenbach, 1979) that ignores the volume of the actin filaments, the activity of actin, and the swelling of the reservoir [$L(t) = L_0 + z\sqrt{4D_a t}$ is plotted with z as in Eq. 2. L_0 was added to Eq. 1 to allow comparison to the simpler models, which are singular for $L_0 = 0$.] Our simpler diffusion-only model (Eq. 7), with the same flawed features, gives curve (a). The two models have nearly identical predictions for these parameters, justifying the simplifying assumptions that we have made.

Fig. 3 shows the experimental data, curve (a) from Fig. 2, and curves (c)–(f), which show the effects of including the various corrections to the minimal models. Curve (c) shows the effect of including actin monomer depletion in the reservoir. The effect is small when the process is not long. For curve (d), the reservoir has been allowed to swell to twice its initial volume, halving the initial concentration of actin, and in curve (e), the fluid-accessible volume of the process is reduced to account for the presence of the actin filaments. Each of the curves (c)–(e) shows the effect of one correction; the combined effect of all three corrections is shown by curve (f). All of the predictions of these models fall below the experimental data.

THE ACTIN RECONCENTRATION MODEL

Effects of water movement

The doubling in volume of the periacrosomal region at the onset of the acrosomal reaction suggests that water movement is an important feature of this system. The Actin Reconcentration Model quantifies how water movement can affect actin delivery and process extension speed.

At the beginning of the acrosomal reaction, ion channels open and allow salt into the periacrosomal region. Water follows, and the periacrosomal region doubles in volume. We assume that the channels eventually return to their

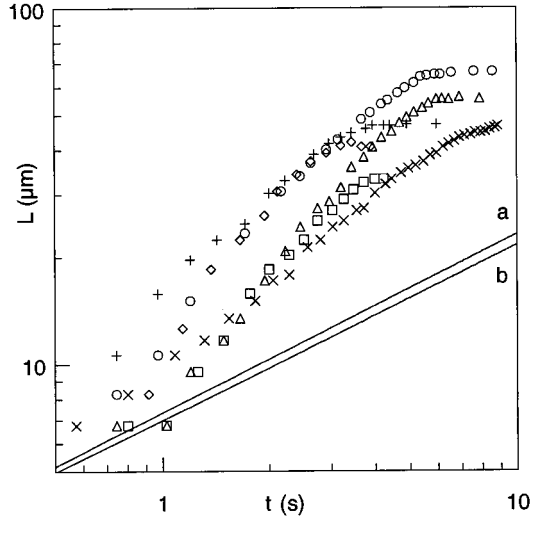

FIGURE 2 Plots of length of the acrosomal process (μm) versus time (s) for the diffusion-only models using parameters from Table 1 and experimental data from Fig. 2 of Tilney and Inoué (1982). We keep the original lettering for the experimental data: B (○), J (◇), D (+), C (△), F (□), and A (×). Curve (a) is the result of Eq. 7, and curve (b) is the result of an earlier model based on Hermans' equation (Eq. 1) (Tilney and Kallenbach, 1979).

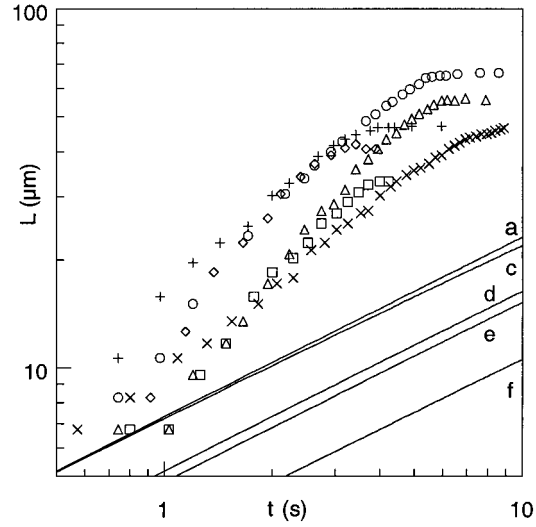

FIGURE 3 Plots of length of the acrosomal process (μm) versus time (s) for theory and experiment. The data and curve (a) are as in Fig. 2. Curves (c)–(e) show the effect of various corrections: depletion of actin monomers from the reservoir (c), initial swelling of the reservoir (d), volume occupation by actin filaments in the process (e). The combined effect of all three corrections is shown in curve (f).

initial states, and that the normal salt content of the compartment is gradually reestablished by ion pumps.

In the model, we artificially divide the salts in the system into two types: β-salt, whose cations are initially dilute inside the cell, flood in through opened ion channels, and are later pumped out again; and α-salt, whose cations are present in the cell initially and do not enter or leave during the acrosomal reaction. In *Thyone*, the β-cation is thought to correspond to Na^+ (Tilney and Inoué, 1985), and the α-cation is thought to correspond to K^+. The most likely candidate for the ion pump is the Na-K ATPase. This ubiquitous pump exports three Na^+ ions and imports two K^+ ions for each molecule of ATP hydrolyzed, while electroneutrality is preserved by passive anion movement.

As the pumps work to restore the initial salt composition, water leaves the system through the membrane to maintain osmotic equilibrium. Actin in the reservoir becomes more concentrated, and diffusion becomes more rapid. See Fig. 4 for a schematic of the Actin Reconcentration Model.

The simple diffusion-only model in the second section needs only to be adjusted slightly so that the volume of the reservoir changes as ions are pumped out. At $t = 0$, it is assumed that $N_{\beta 0}$ β-salt ions have already entered the periacrosomal region, and water moving to maintain osmotic equilibrium across the membrane has already swollen the region to $V_{\text{res}}(0) = 2V_0$. These processes are not explicitly modeled. As the ions are pumped out, $N_\beta(t)$ decreases, and water leaves the system to maintain osmotic equilibrium. Because the original doubling of the reservoir occurred in only ~60 ms (i.e., a volume V_0 of fluid enters in 60 ms)

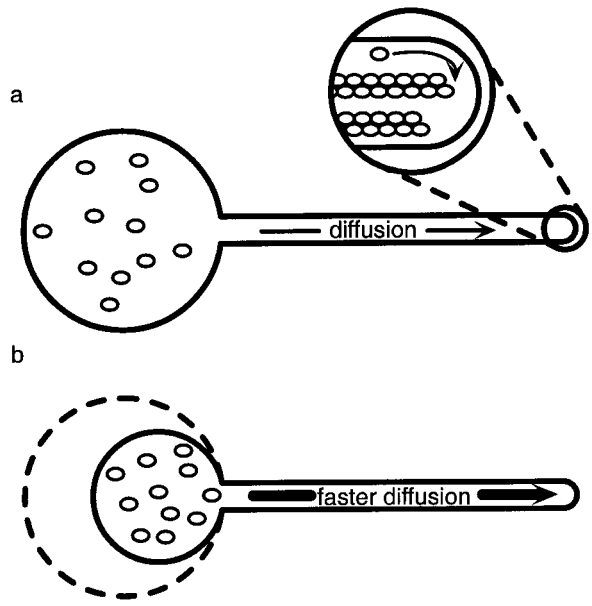

FIGURE 4 Schematic of the Actin Reconcentration Model. (*a*) Actin in solution in the periacrosomal region diffuses to the tip of the process where it is polymerized. When salt ions are pumped out, water follows, causing the reservoir to shrink (*b*). Actin becomes more concentrated, increasing diffusive flux. The process and monomers are shown exaggerated in size compared to the reservoir.

(Tilney and Inoué, 1982), we assume that water can move to equalize osmotic pressure differences infinitely fast as salt is pumped out of the system. Because the process is so thin, we ignore its volume and any solutes within its volume. Therefore the volume of the reservoir is determined by the total number of salt ions within the reservoir:

$$V_{\text{res}}(t) = V_0\left[\frac{N_{\alpha 0} + N_\beta(t)}{N_{\alpha 0}}\right], \tag{11}$$

where $N_\beta(t)$ is the number of excess salt ions remaining in the reservoir, and $N_{\alpha 0}$ is the unvarying number of α-salt ions in the reservoir. The number of β-salt ions in the reservoir is governed by

$$\frac{dN_\beta}{dt} = -S_0 j_\beta, \tag{12}$$

where S_0 is the area of the membrane through which ions are being pumped, and j_β is the flux (in number of ions pumped per time per area) with which salt is pumped through the membrane. Although the reservoir's initial volume is known from experimental work, its initial membrane area must be estimated. In the absence of any experimental data about membrane creation or distribution, the system's total membrane area (reservoir plus process) is assumed constant.

As a simple approximation to the workings of an ion pump, we take the flux of ions j_β through the membrane to be

$$j_\beta = j_{\beta\text{-max}}\left(\frac{c_\beta}{c_\beta + c_{\beta,1/2}}\right), \tag{13}$$

where c_β is the concentration in the reservoir of the ions being pumped, $j_{\beta\text{-max}}$ is the maximum capacity of the pumps, and $c_{\beta,1/2}$ is the concentration at which the ion pumps operate at half of their maximum capacity. The concentration of ions is $c_\beta = N_\beta/V_{\text{res}}$, where the volume of the reservoir is now a function of time. Equation 12 then becomes

$$\frac{dN_\beta}{dt} = -S_0 j_{\beta\text{-max}}\frac{N_\beta}{N_\beta + c_{\beta,1/2}V_{\text{res}}}. \tag{14}$$

With $N_\beta(0) = N_{\beta 0}$, Eqs. 11 and 14 can be solved numerically for V_{res}.

The only adjustment that then needs to be made to Eq. 9 is to replace $(2V_0)$ by V_{res}:

$$\frac{dL}{dt} = \frac{D_a A_d}{V_{\text{res}}}\frac{(1 - L/L_\infty)}{L/L_\infty}. \tag{15}$$

This equation cannot be integrated, but it can again be solved numerically by *Mathematica* (Wolfram, 1996).

Effects of nonideality

Our second modification in the Actin Reconcentration Model is to the driving force for diffusion. Because the

volume fraction of protein is very high in this system, the nonideality of actin is significant. We replace the concentration of actin with its activity:

$$c_a \rightarrow a_a = \gamma_a c_a, \tag{16}$$

where a_a is the activity of actin and γ_a is the activity coefficient of actin. The activity coefficient is derived from the chemical potential μ_a via $\gamma_a = a_a/a_{a,id} = \exp(\mu_a - \mu_{a,id}/k_BT)$, where $a_{a,id}$ and $\mu_{a,id}$ are the ideal activity and chemical potential, respectively. According to scaled particle theory (Han and Herzfeld, 1994), the chemical potential of a monodispersed hard sphere fluid is

$$\frac{\mu_a}{k_BT} = \ln(c_a\Lambda_a^3) - \ln(1-\varphi_a) + 7\left(\frac{\varphi_a}{1-\varphi_a}\right) + \frac{15}{2}\left(\frac{\varphi_a}{1-\varphi_a}\right)^2 + 3\left(\frac{\varphi_a}{1-\varphi_a}\right)^3, \tag{17}$$

where Λ_a is the thermal wavelength of actin, $\varphi_a = c_a\nu_a$ is the volume fraction of actin, and ν_a is the volume of an actin monomer. The ideal value is obtained in the limit $\varphi_a \rightarrow 0$, and the activity coefficient is

$$\gamma_a(\varphi_a) = \frac{1}{(1-\varphi_a)}\exp\left[7\left(\frac{\varphi_a}{1-\varphi_a}\right) + \frac{15}{2}\left(\frac{\varphi_a}{1-\varphi_a}\right)^2 + 3\left(\frac{\varphi_a}{1-\varphi_a}\right)^3\right]. \tag{18}$$

With the replacement of the actin concentration $c_a = (N_{a0}/V_{res})(1 - L/L_\infty)$ by the activity $a_a = c_a\gamma_a(\varphi_a) = c_a\gamma_a(c_a\nu_a)$, Eq. 15 becomes

$$\frac{dL}{dt} = \frac{D_a A_d}{V_{res}}\frac{(1-L/L_\infty)}{L/L_\infty}\gamma_a\left(\frac{N_{a0}(1-L/L_\infty)}{V_{res}}\nu_a\right). \tag{19}$$

As before, this equation can be solved numerically by *Mathematica* (Wolfram, 1996).

Choice of parameter values

Table 2 summarizes the values of the parameters used in the Actin Reconcentration Model that are not included in Table 1. The number of ions pumped across the membrane depends on its surface area. At least 1.4×10^{-7} cm^2 of membrane must be present to cover a 0.05-μm diameter, 90-μm-long cylindrical process. This is more than is required to encompass the initial reservoir after swelling (but before the process is constructed). The final volume of the periacrosomal region is not experimentally known, but in the Actin Reconcentration Model, it reaches a final volume close to its pre-doubling volume V_0. About another 3.1×10^{-8} cm^2 of membrane would be needed to cover a sphere of $V_0 = 5.1 \times 10^{-13}$ cm^3. We use an initial membrane area 15% larger than the sum of the membrane needed to cover the process and reservoir separately: $S_0 = 2 \times 10^{-7}$ cm^2.

TABLE 2 Additional parameter values for the Actin Reconcentration Model

Symbol	Parameter	Value
S_0	Initial reservoir surface area	2.0×10^{-7} cm^2
$j_{\beta\text{-max}}$	Maximum ion flux	3.0×10^{14}/(cm^2 · s)
$c_{\beta,1/2}$	Ion concentration at half-maximum flux	17 mM
Π_{ext}/k_BT	External osmotic pressure	1 M
$N_{\beta 0}$	Number of ions entering during swelling	3.06×10^8
$N_{\alpha 0}$	Initial number of ions in the reservoir	3.06×10^8
ν_a	Volume of profilin-actin complex	6.9×10^{-20} cm^3

We estimate the rate of ion pumping from experimental data. The maximum reported turnover for Na-K ATPases is $\sim 5 \times 10^{13}$ ATP/(cm^2 · s) in rat soleus muscle (Sejersted, 1988). Assuming net movement of three Na^+ ions and three accompanying anions per ATP hydrolyzed (while higher K^+ permeability yields no net K^+ transport), this turnover corresponds to a net flux of ions moving across the membrane of $j_{\beta\text{-max}} = 3 \times 10^{14}$ ions/(cm^2 · s). The maximum ion flux could be higher, because neither the density of the pumps in this membrane nor their maximum turnover rate is known. The other parameter controlling ion transport, the concentration at half rate $c_{\beta,1/2}$, is set to 17 mM. The value of $c_{\beta,1/2}$ affects the rate at which the ion transport falls with decreasing salt concentration, but the extension rate of the process is insensitive to the value of $c_{\beta,1/2}$ as long as it is sufficiently small.

The external osmotic pressure Π_{ext}/k_BT is set to 1 M, approximately the osmotic pressure of seawater (Lide, 1998), the natural environment of a sea cucumber. The number of ions initially present in the reservoir (α-salt ions) can be calculated by assuming that the periacrosomal region is in osmotic equilibrium prior to the acrosomal reaction. Given the (pre-doubling) volume, we calculate that there must be $N_{\alpha 0} = 3.06 \times 10^8$ ions present to balance the external osmotic pressure. When the acrosomal reaction is triggered, β-cations enter, and anions follow. Assuming that something close to a state of osmotic equilibrium is attained after the doubling, an influx of $N_{\beta 0} = 3.06 \times 10^8$ ions would be required to balance the external osmotic pressure in the added volume ($N_{\beta 0}/V_0 = \Pi_{ext}/k_BT$).

The activity coefficient of the profilin-actin complex is calculated using Eq. 18, which requires the complex's molecular volume ν_a. Again assuming a density of 1.4 g/cm^3, the profilin (16 kDa)-actin (42 kDa) complex would have a volume of $\sim\nu_a = 6.9 \times 10^{-20}$ cm^3 = (4.1 nm)^3.

Results

As in the second section, the theoretical results are compared with the experimental data of Tilney and Inoué (1982). Unless otherwise noted, the parameters in Tables 1 and 2 were used in calculating the results of the Actin Reconcentration Model.

Fig. 5 shows the effect of including pumping and nonideality in the model. Fig. 5 *b* is identical to Fig. 5 *a* except

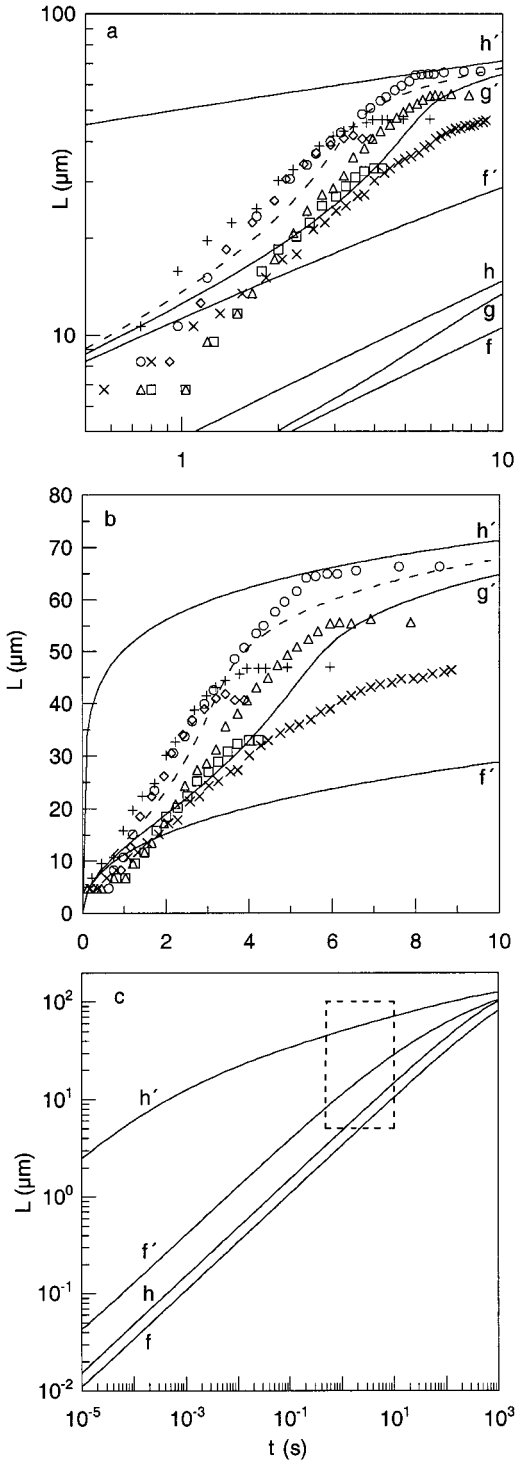

FIGURE 5 Plots of length of the acrosomal process (μm) versus time (s) for theory and experiment on (*a*) log-log and (*b*) linear-linear scales, and (*c*) an expanded log-log scale. The data are as in Figs. 2 and 3, and curve (f) is as in Fig. 3. Curves (g) and (h) show results for the Actin Reconcentration Model ignoring nonideality (the solution to Eq. 15). Curve (h) was calculated assuming effectively infinitely fast ion pumping. The infinitely fast pumping negates the effects of the initial swelling. Curve (g) was calculated with $j_{\beta\text{-max}} = 3 \times 10^{14}$ ions/(cm^2 · s), i.e. the unprimed curves are omitted in *b*. Curves (f′)–(h′) were calculated including the effects of solute nonideality (the solution to Eq. 19), with parameters that are otherwise the same as for the unprimed curves. The dashed curve is the same as curve (g′), except the pump rate has been increased to $j_{\beta\text{-max}} = 5 \times 10^{14}$ ions/(cm^2 · s). Panel (*c*) was calculated with a smaller L_0 than the other panels so as to better resolve the behavior at small *t*. The large *t* behavior is unaffected by using a smaller L_0. The dashed box in (*c*) is the plot area shown in panel (*a*).

that *b* is plotted on a linear-linear scale, and the unprimed curves are omitted. The first (unprimed) set of curves in Fig. 5 *a* shows the effects of pumping while preserving ideality (solution of Eq. 15). Curve (f) is the same as in Fig. 3, showing the corrected diffusion-only model (i.e., $j_{\beta\text{-max}} = 0$). Curve (h) was calculated with $j_{\beta\text{-max}} = 10^{26}$ ions/(cm^2 · s). That value is chosen to be sufficiently large that the pumps are effectively infinitely fast. Because the initial swelling of the reservoir is counteracted immediately, this case is equivalent to a "no swelling" scenario. The extension rate is increased due to the increased concentration of actin monomers in the unswollen reservoir. Curve (g) was calculated with the physiological $j_{\beta\text{-max}} = 3 \times 10^{14}$ ions/(cm^2 · s). It falls neatly between curves (f) (no pumping) and (h) (infinitely fast pumping), reflecting that as ions are pumped out, the reservoir volume decreases from 2 V_0 to $\sim V_0$. The predictions, however, still fall well below the experimental data.

The effects of nonideality are added to the model in the primed curves in Fig. 5, *a* and *b*. These curves represent the solution to Eq. 19 with the same parameters as for the corresponding unprimed curves. The sole difference is the inclusion of nonideality in the primed curves. The broken line is the same as curve (g′), but with a slightly higher pump rate: $j_{\beta\text{-max}} = 5 \times 10^{14}$ ions/(cm^2 · s).

The data and the models each have a characteristic $L(t)$ shape. The experimental data have been characterized as falling on a straight line when plotted as L^2 vs. t (Tilney and Inoué, 1982). On a log-log plot (Fig. 5 *a*), such a curve would be straight. However, it is clear in Fig. 5 *a* that the experimental data generally have a concave-down shape. Furthermore, in some of the trials, sigmoidicity can be seen at shorter times. The linear-linear plot, Fig. 5 *b*, provides a more realistic representation for short times, where measurements of shorter processes entail larger relative errors.

Some of the calculated curves ((f), (f′), (h), and (h′)) in Fig. 5 *a* appear to be straight. This is an artifact of plotting the curves only over experimentally relevant times (0.5–10 s). In fact, all of these curves have a downward concavity at large *t*, due to depletion of monomers in the reservoir. This can be seen when they are plotted over a wider time interval (Fig. 5 *c*). In the models corresponding to these curves, the reservoir volume is constant, either due to no ion pumping (curves (f) and (f′)) or infinitely fast ion pumping (curves (h) and (h′)). When the reservoir volume is constant and nonideality is not included (curves f and h), the governing differential equation is Eq. 9, whose solution is Eq. 10 (although curve (h) was generated via Eq. 15 with an "infinite" pump rate). When the process length L is small, $t(L)$ in Eq. 10b is well-approximated by the first term ($m = 2$) in the series, and the $L^2 \sim t$ form of Eq. 7 is recovered.

So in Fig. 5 *c*, (f) and (h) are essentially straight with slope 2 at small t, and it is only at larger t that the downward concavity can be seen. Even then, the curvature is small. However, when nonideality is included, as in curves (f′) and (h′), the same approximation does not hold, and the downward concavity occurs most visibly at shorter times than those plotted in Fig. 5, *a* and *b*.

The effects of varying the parameters in the model can also clearly be seen in Eq. 10b. Increasing either the diffusion coefficient D_a or the area available for diffusion A_d results in a shorter time to reach the same length (faster growth). Increasing the reservoir volume V_0 has the opposite effect, because a larger reservoir volume translates to a lower concentration of actin, and therefore a shallower concentration gradient to the tip. The parameter L_∞, which is proportional to the number of actin monomers N_{a0} initially present in the reservoir, occurs strictly in the denominator because the series starts with $m = 2$. Increasing L_∞ corresponds to increasing the actin concentration and therefore decreases the time needed to reach a given length.

The curves in Fig. 5 *a* corresponding to the Actin Reconcentration Model, (g), (g′), and the broken line, have a sigmoid shape. The position of the downward concavity in the calculated curves, which appears at longer times as in the data, is controlled in large part by the product of the ion pump rate $j_{\beta\text{-max}}$ and the system's membrane surface area S_0. Much of the experimental data can be bracketed by curve (g′) and the broken curve, corresponding to $j_{\beta\text{-max}} = 3$ and 5×10^{14} ions/(cm^2 · s) respectively, with all of the other parameters held constant. The point in the Actin Reconcentration Model where the slope begins to flatten corresponds roughly to the point where the reservoir stops changing volume because salt concentrations have been restored.

Most of the other parameters in the model affect the overall magnitude and position of the $L(t)$ curve more than its shape. Note that dL/dt in Eq. 15 is the growth rate. Therefore, increasing either D_a or A_d will increase the growth rate, just as discussed above with respect to Eq. 10. Increasing L_∞ has the same effect. Any of these increases in the growth rate tend to move the $L(t)$ curve upward. Also, as mentioned above, the product $j_{\beta\text{-max}}S_0$ controls the position of the inflection in the $L(t)$ curve, but an increase in that combination also increases the growth rate and moves the $L(t)$ curve up, because a larger $j_{\beta\text{-max}}S_0$ results in a V_{res} that decreases faster.

The behavior of variables other than $L(t)$ better illustrates the relationship between ion pumping and process growth. Fig. 6 *a* shows plots of the number of β-salt ions (N_β), the volume of the reservoir (V_{res}), the concentration of actin monomers (c_a), and the process length (L) as a function of time in the Actin Reconcentration Model, using the parameters for curve (g′) in Fig. 5. The salt in the reservoir drops steadily due to the action of the ion pumps until $\sim t = 5.5$ s, at which time nearly all of the excess ions have been pumped out of the system. The volume of the reservoir shrinks in direct correlation to the number of β-salt ions.

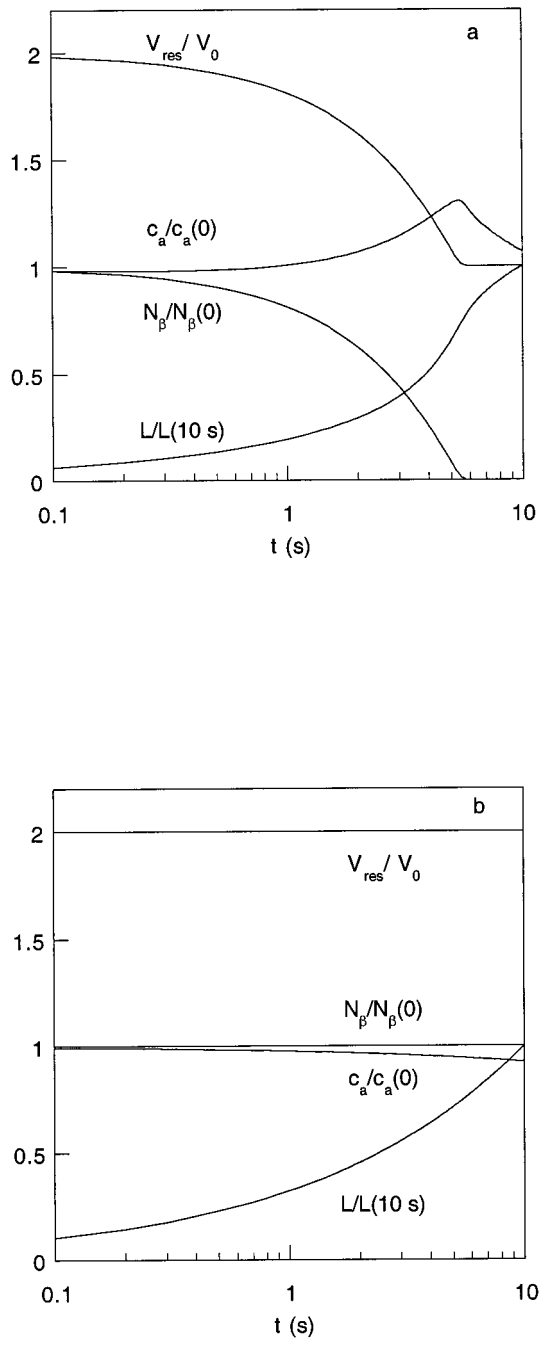

FIGURE 6 Reservoir behavior in the Actin Reconcentration Model: the volume of the reservoir (V_{res}), scaled by its pre-swelling value; the concentration of actin monomers in the reservoir (c_a), scaled by its initial value; the concentration of excess ions in the reservoir (c_β), scaled by its initial value; and the length of the acrosomal process (L), scaled by its final value. The curves in (*a*) were calculated in the Actin Reconcentration Model using the same parameters as were used to generate Fig. 5, curve (g′). In panel (*b*), neither ions nor water are transported across the membrane. The parameters are the same as were used to generate Fig. 5, curve (f).

The concentration of actin monomers in the reservoir rises as the volume shrinks. Therefore, the driving force for actin delivery also increases. The effects can be seen in the upward bend in $L(t)$ at $\sim t = 3$–5 s. At $\sim t = 5.5$ s, $V_{res}(t)$

plateaus because no more excess salt is left to be pumped out. The concentration of actin monomers no longer rises due to the shrinkage of the reservoir. Rather, it begins to fall, as monomer depletion due to polymerization is no longer masked by the reconcentration of actin due to reservoir shrinkage. At this point, $L(t)$ turns downward again. When ion transport is turned off (diffusion-only model), most of these effects are absent. Fig. 6 *b* shows the same curves as Fig. 6 *a* when ion pumping has been turned off. The reservoir's volume remains constant, so the actin concentration in the reservoir drops due to polymerization rather than rising due to reservoir shrinkage.

RELAXATION OF ASSUMPTIONS

Method

Numerical methods allow us to relax some of the assumptions made above and assess their validity. The mathematical base of this approach is the continuity equation. Because the process is very narrow (~50 nm in diameter) compared to its length (30–90 μm) (Tilney and Inoué, 1982), lateral diffusion quickly levels any lateral concentration gradients. Therefore, the concentration of actin monomers and salt ions can be considered constant across the process diameter, and gradients occur only along the process. Fluid flow in the process is also assumed to be one-dimensional. Instead of solving the full low Reynolds number hydrodynamic equations, the fluid speed is assumed to be uniform over the cross-sectional area of the process, although varying along its length. The one-dimensional continuity equation for the solutes is then

$$\frac{\partial c_i(x,t)}{\partial t} + \frac{\partial j_i(x,t)}{\partial x} = 0, \tag{20}$$

where $c_i(x,t)$ are the solute concentrations, $j_i(x,t)$ are the solute fluxes (in particles per area per time), and $i = a$, α, and β refers to actin and the two varieties of salt, respectively. The fluxes arise from diffusion and bulk flow:

$$j_i = -D_i(\partial a_i/\partial x) + \upsilon c_i, \tag{21}$$

where D_i is the diffusion coefficient of the ith species, υ is the speed of the movement of fluid in the process, $a_i = \gamma_i c_i$ is the activity of the ith species, and γ_i is the activity coefficient of the ith species. In practice, we make the approximation that the salt ions are ideal solutes: $a_\alpha = c_\alpha$ and $a_\beta = c_\beta$.

We must also add sink terms Λ_i to the continuity equation to account for particles that leave the solution through polymerization (actin) or active transport (β-salt).

$$\frac{\partial c_i}{\partial t} + \frac{\partial j_i}{\partial x} = \Lambda_i \tag{22}$$

If we assume that the fluid speed varies slowly along the process, the continuity equation then takes the form

$$\frac{\partial c_i}{\partial t} + \upsilon\frac{\partial c_i}{\partial x} - D_i\frac{\partial^2 a_i}{\partial x^2} = \Lambda_i, \tag{23}$$

Because this equation is an expression of the conservation of mass, it holds everywhere in the process. The α-salt ions do not enter or leave the process, so $\Lambda_\alpha = 0$ everywhere. Λ_β accounts for the loss of ions through the action of ion pumps. It can be easily calculated using Eq. 13 (see the Appendix for details).

For actin, $\Lambda_a \neq 0$ only at the tip of the process where polymerization takes place. Λ_a is proportional to the polymerization rate, which is proportional to the extension speed dL/dt. Unlike the earlier models, in which actin was assumed to polymerize infinitely fast, in this model the rate of actin polymerization is given by the Brownian Ratchet Model (Peskin et al., 1993) of force transduction (see Fig. 7). In the Brownian Ratchet Model, polymerization "ratchets" membrane fluctuations into unidirectional motion. When the ends of actin filaments abut the cell membrane, polymerization is blocked. However, fluctuations of the membrane may open gaps between the filament and the membrane, allowing polymerization to occur. Then the membrane cannot return to its original position due to the presence of the now-longer filament. In the range of parameters relevant to this system, the Brownian Ratchet Model predicts an extension speed dL/dt of

$$dL/dt = \delta(k_+ a_{a,\mathrm{tip}} e^{-\omega} - k_-), \tag{24}$$

where $k_+(k_-)$ is the on (off) rate constant for actin polymerization, and $\omega = f\delta/k_B T$, where k_B is Boltzmann's constant, T is the absolute temperature, and f is the force on each filament opposing elongation. The Brownian Ratchet

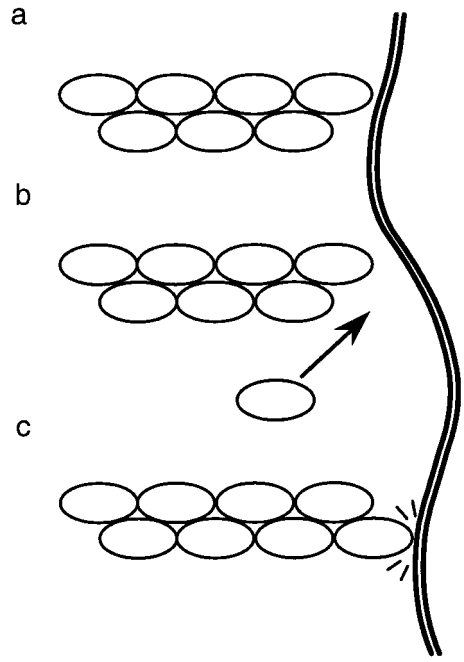

FIGURE 7 A schematic of the Brownian Ratchet Model (Peskin, et al., 1993). (*a*) An abutting membrane hinders polymerization, but (*b*) Brownian fluctuations can create membrane-filament gaps large enough for a monomer to be added; after which (*c*) the membrane cannot return to its original position: the "ratchet."

is not a critical part of our model. We chose the Brownian Ratchet Model as a convenient way to quantitatively relate extension speed to local monomer concentration and opposing force, but any quantitative model for protrusion would suffice. The details are unimportant, because extension speed is limited by actin delivery, not polymerization rate or membrane tension. However, including a finite polymerization rate allows us to test the initial assumption of infinitely fast polymerization.

The analytical model presented in the previous section did not include one effect of allowing water to move through the process membrane: the effects of bulk fluid flow within the process. The speed v of the fluid flow in Eq. 23 is not in general equal to the extension speed of the process. It is also determined by how much water leaves the process through the membrane. Because the actin filaments that form the core of the acrosomal process prevent the process's membrane from collapsing, escaping water must be replaced from elsewhere in the system: ultimately from the periacrosomal region, which has no actin filament framework and is free to shrink as fluid leaves it. At any given location in the process, the fluid speed is determined by the volume of fluid that passes that point on its way from the periacrosomal region to the rest of the process, either to fill the growing process or to replace water that has left the process through the membrane. This volume is divided by the cross-sectional area of the process and the time interval to give the fluid speed at that point in the process. This bulk flow potentially transports more actin to the tip of the process, but because the membrane area of the reservoir is far larger than that of the process (at least during the early stages of growth), relatively little water leaves the process, and little actin is transported in this manner. By the time the process's membrane area becomes appreciable, β-salt pumping is finished, and no more water leaves the process. Then the fluid speed in the process is the same as the process extension speed.

In general, the flux j_w of water molecules through a membrane due to an osmotic pressure difference is given by Katchalsky and Curran (1967) and Macey and Brahm (1989)

$$j_w = P_w \Delta\Pi, \tag{25}$$

where P_w is the hydraulic permeability coefficient of the membrane. $\Delta\Pi$ is the osmotic pressure difference across the membrane:

$$\Delta\Pi = \Pi_{ext} - c_\alpha - c_\beta, \tag{26}$$

where Π_{ext} is the osmotic pressure of the medium outside the process membrane. Even taking the nonideality of actin into account, the two cation types and their accompanying anions can be assumed to contribute almost all of the osmotic pressure inside the process.

The system of equations is nonlinear (especially due to the form of γ_a) and impossible to solve analytically. Our approach is therefore to discretize the continuity equation (Eq. 23) and to iterate the equations on a computer. Complete details of the discretization are contained in the Appendix.

Choice of parameter values

Table 3 summarizes the values of the parameters used in the iterative version of the Actin Reconcentration Model that are not included in the previous two tables. For convenience, we choose a diffusion coefficient of $D_\beta = D_\alpha = 1.5 \times 10^{-5}$ cm^2/s for all the salt ions, which lies within the range of values for Na^+, K^+, and Cl^- (Stein, 1990).

Monomeric actin is added to the actin filament directly from the profilin-actin complex. This is thought to occur at least as rapidly as actin polymerization without profilin (Pantaloni and Carlier, 1993; Pring et al., 1992). We therefore use the in vitro on- and off-rate constants for actin polymerization: $k_+ = 11.6\ (\mu M \cdot s)^{-1}$ and $k_- = 1.4\ s^{-1}$ (Pollard, 1986). In the Brownian Ratchet Model, the filament ends grow against an opposing force, in this case, the membrane tension. Peskin et al. (1993) quote a value of $\sigma = 0.035$ dyne/cm for a typical membrane tension, so the load force per fiber of $f = 2\pi r\sigma/N_f \approx 0.1$ pN is appropriate for the acrosomal process. In any case, the final extension rate is limited not by the polymerization rate but by the rate of actin monomer delivery, so the extension rate is almost entirely insensitive to the choices of k_+, k_-, and f under physiologically relevant conditions. The temperature T, also required for the Brownian Ratchet Model, is set to $T = 300$ K (room temperature).

The hydraulic permeability P_w of the membrane can be estimated from observations of the doubling of the periacrosomal region. Because the solute concentrations inside and outside the compartment, the initial and final volumes, and the length of time to change volume (50–70 ms (Inoué and Tilney, 1982)) are all known, it is possible to integrate Eq. 25 over time and find a permeability that is consistent with the experimental observations: $P_w = 5.2 \times 10^{-2}$ cm/s. That permeability is about seven times the permeability of a red blood cell (Macey and Brahm, 1989), and about one-third the permeability of proximal tubules in rabbit kidneys (Agre et al., 1993). While large, it falls within the range of permeabilities exhibited by other biological membranes. As the sperm has no other function than to fertilize the egg, it

TABLE 3 Additional parameter values used in iterative model

Symbol	Parameter	Value
D_α, D_β	Ion diffusion coefficients	1.5×10^{-5} cm^2/s
k_+	Actin on-rate constant	$11.6/(\mu M \cdot s)$
k_-	Actin off rate	1.4/s
f	Load force per filament	0.1 pN
T	Temperature	27°C (300 K)
P_w	Membrane water permeability	5.2×10^{-2} cm/s
ℓ	Segment length	0.1 μm
Δt	Time step	0.2 μs

is not implausible that its membrane may be especially water-permeable for the purpose of driving elongation of the acrosomal process.

The size of the segments over which the equation was discretized was chosen to clearly resolve the structure of the concentration profiles. We used a segment size of $\ell = 0.1$ μm length throughout. A time step of $\Delta t = 0.2$ μs is adequate to maintain stability of the iteration at that segment size. Further reduction in the time step or segment size has little effect on the results. As before, the initial length of the process L_0 is set to 0.19 μm. This length extends beyond one segment but does not place the process's end at a boundary or a center (multiples of ℓ and $\ell/2$ are both special cases for our algorithm; see the Appendix for details).

Results

The model described in this section can calculate results corresponding to all of the models in the second and third sections. Ion transport can be disabled by setting $j_{\beta\text{-max}} = 0$, and water movement can be prevented by making the membrane impermeable to water ($P_w = 0$). Unless otherwise noted, the parameters in Tables 1–3 were used in calculating the results of the models.

Fig. 8 shows $L(t)$ plots for a variety of parameters and models. Each label indicates a pair of curves, one calculated by the full computer-solved model (*dashed lines*), and the other by the simpler analytic models (*solid lines*) from the previous sections. The solid lines have all appeared in previous figures, and their labels have not changed. Curve (a) corresponds to the uncorrected model from the second section and curve (f) to the corrected model from the same section. Curve (g′) is the prediction of the model that includes nonideality and ion pumping, with a pump rate of $j_{\beta\text{-max}} = 3 \times 10^{14}$ ions/(cm^2 · s).

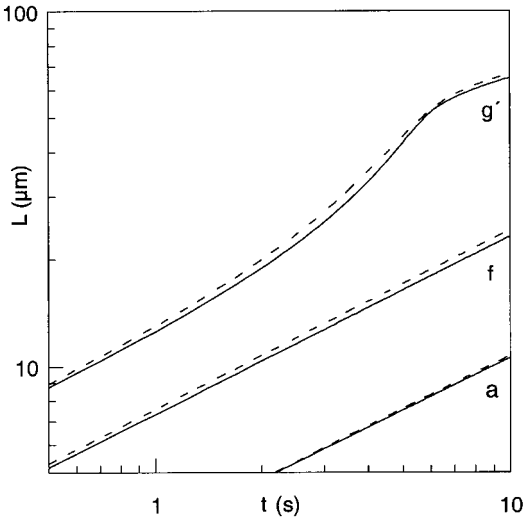

FIGURE 8 Comparison of $L(t)$ predictions of the simpler analytical models of the second and third sections (*solid lines*) with the predictions of the more elaborate computer-based model of the fourth section (*dashed lines*). Each labeled set of curves contains both a solid and dashed line, even if they are not distinguishable. Curves (a), (f), and (g′) are as in Figs. 2, 3, and 5, respectively. In all cases, the predictions of the two methods are nearly identical.

In each case, the predictions of the simpler analytic model (*solid line*) and the computer-based model (*dashed line*) lie nearly on top of one another. Thus, the models of the second and third sections semi-quantitatively reproduce the results of the full computer model, justifying the approximations that we made in those sections, including infinitely fast polymerization, linear activity profiles, and one-dimensional diffusion without bulk fluid flow.

Fig. 9 *a* shows the concentration of actin in the process at four times during the extension of the process. These data come from the computer-solved version of the Actin Reconcentration Model with the parameters in Tables 1–3 (corresponding to the *dashed line* of curve (g′) in the previous figure). The four profiles correspond to $t = 2.5$, 5, 7.5, and 10 s after the process begins to grow. They are not the flattened profile with an exponential drop-off one might expect for a diffusive system with significant bulk flow, because the overall bulk flow in this system is small. Nor are they the linear profiles one would expect between two endpoints maintained at different concentrations, because the driving force for diffusion is the activity of actin, not the concentration. The concentration profiles shown do, however, translate to activity profiles that are nearly linear (Fig. 9 *b*), providing evidence that our assumption in the second and third sections of linear activity profiles at all times was a good one.

DISCUSSION

The question of whether or not diffusion-based actin transport is sufficient to support the observed extension speed of the *Thyone* acrosomal process has been answered first in the positive (Tilney and Kallenbach, 1979) and later in the negative (Perelson and Coutsias, 1986). Other models have also been proposed. Oster et al. (1982) suggested that after the periacrosomal region doubles in volume, the walls of that region, elastically stretched, would push the fluid forward, extending the process by hydrostatic pressure. The actin core would not extend with the process, but catch up later. The slow rate of actin monomer delivery would therefore not limit the growth of the process. The calculations obtain experimental speeds, by fitting some model parameters to the data, rather than independently determining them. Moreover, hydrostatic pressure equalizes at about the speed of sound in a fluid, and it is therefore unclear why the membrane tension after swelling should be greater at the rear of the process than at the front, as would be necessary to cause elongation. In another paper, Oster and Perelson (1987) suggest that the osmotic movement of water into the acrosome through the membrane at the process's tip may assist in extending the acrosomal process by "inflating" it with fluid. But they provide no plausible driving force for this influx, and they also note correctly that such an influx

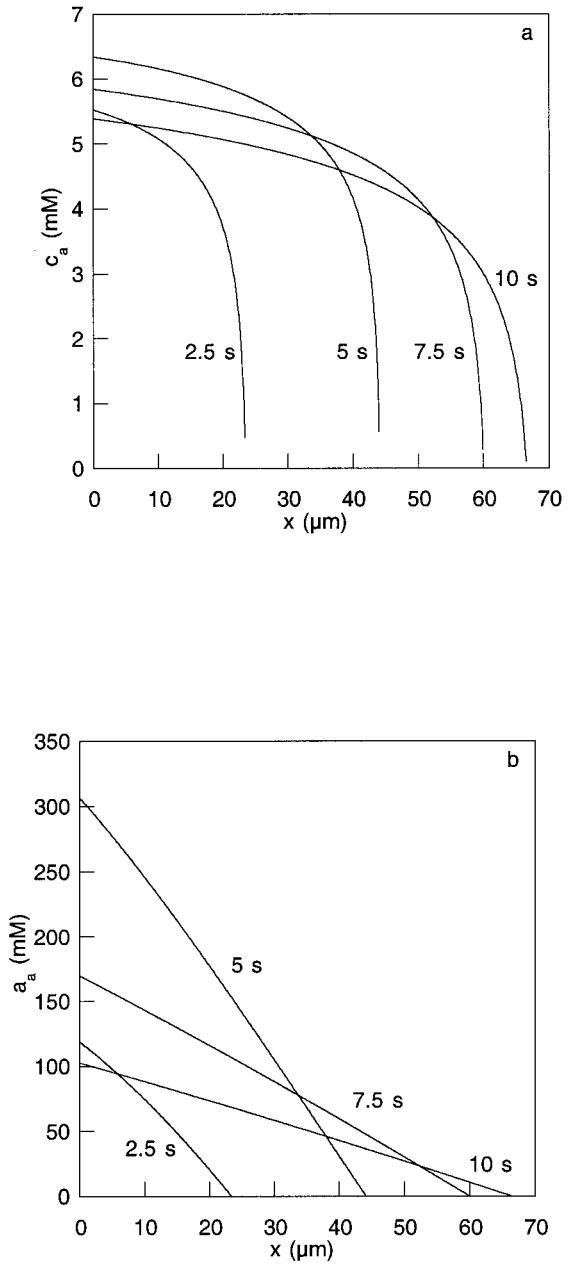

FIGURE 9 Plot of the concentration (*a*) and activity (*b*) of actin (mM) as a function of position in the process (μm) for the iterative computer version of the Actin Reconcentration Model. The parameters correspond to those used for curve (g′) in Fig. 5. The four curves correspond to snapshots at 2.5, 5, 7.5, and 10 s after the beginning of the acrosomal reaction.

of fluid would interfere with monomer delivery to the tip. Zhu and Skalak (1988) used their model of pseudopod protrusion to describe the extension of the acrosomal process. In that model, actin monomers travel by both diffusion and fluid flow, the fluid being driven forward to fill the growing tip. Unfortunately, the model parameters are not independently evaluated, and the central part of the growth curve is fit by scaling the length and adjusting the zero of time.

In this model we have tried to incorporate more biological detail than was present in earlier diffusion-only models, and we have used only parameters whose values can be found in the literature. While *Thyone* data may not be available for every parameter (e.g., ion pump characteristics), the literature contains plausible baseline values for every parameter from other systems.

Limitations and approximations

In our calculations, we have made a number of approximations that, we believe, simplify the system to a level that is manageable without losing its essential elements. Nonetheless, we will examine the approximations and the expected results were they to be removed.

Some of the approximations made in the second and third sections were drastic: infinitely fast polymerization, $c_{a,tip} = 0$, equilibrium (linear) activity profiles, and infinitely fast water movement. Often the process was ignored compared to the periacrosomal region, which has greater volume, surface area, and solute content. As demonstrated by the close agreement with the previous section's computer-solved model (which removed those assumptions), these approximations are all justified.

In the previous section, when calculating the flow of fluid forward from the periacrosomal region to the tip of the acrosomal process, we simply calculated the volume of water that had escaped the extension and required that the same volume be drawn in from the reservoir to the rear. The volume drawn in was spread over the cross-sectional area of the extension to give a flux. The fluid flow may in fact be *very* different from what we describe. Because the actin filaments are fairly close together and the concentration of actin monomers is fairly high, the system may more closely resemble a set of actin "balls" rattling around in a lattice of parallel actin "wires" rather than solute in smooth fluid flow. A detailed hydrodynamic calculation (a difficult proposition) would account for these effects. However, because bulk flow plays such a small role in the Actin Reconcentration Model, the effect of a more detailed treatment of hydrodynamic effects is expected to be very small.

We have assumed throughout that diffusion coefficients do not vary with solute concentration, when it is known that self-diffusion coefficients decrease when concentration increases (Han and Herzfeld, 1993; Muramatsu and Minton, 1988). However, unlike other cells, most of the protein in the acrosomal process is actin, and therefore mutual diffusion is more relevant than self-diffusion. The presence of some higher molecular weight proteins and some free profilin has been ignored in our models. Although these proteins will slow actin diffusion somewhat, they will also increase the solute activity, which is the driving force for diffusion (Han and Herzfeld, 1994). Thus the decrease in the diffusion coefficient due to crowding by other solutes is at least partially offset by the increased driving force (activity) due to the same crowding, and a more rigorous examination of diffusion in such a concentrated mixture is beyond the scope of this paper.

Termination of process growth

In the course of trying to answer how the acrosomal process can reach 60–90 μm in 10 s, it became clear that a second question is also important: why does the process stop growing? Experimentally, the length of the process increases steeply but then suddenly plateaus. The sharpness of the crossover suggests a definite mechanism or condition for halting. By itself, depletion of actin from the system results in a gradual decrease in extension speed as the actin concentration gradually falls.

Depletion of membrane may halt process growth. Once all of the available membrane in the system has been distributed to cover the process and reservoir, polymerization at the tip would face increasing resistance, eventually stopping when the membrane can no longer deform enough to add another monomer. (This corresponds to reaching the "stall force" of the Brownian Ratchet Model: the force at which $dL/dt \rightarrow 0$ in Eq. 24.)

Effects of osmotic pressure variation

The effects of hyperosmotic and hypoosmotic conditions on the growth of the acrosomal process of *Thyone* have been experimentally probed by Tilney and Inoué (1985). In brief, they found that hyperosmotic conditions tended to suppress growth of the acrosomal process, with no growth at all found at 150% of normal tonicity. The opposite effect was also seen to hold: a decrease in external osmotic pressure increased the extension rate. A straightforward qualitative interpretation of these results is that actin monomer release in the initial reaction is correlated with the degree of swelling of the periacrosomal region. Unfortunately, no detailed modeling of these experiments can be made without knowing either the volume of water or the amount of salt that enters the periacrosomal region under the altered osmotic conditions.

Experimental tests

Thyone sperm is not very amenable to internal manipulation, either before or during the acrosomal reaction, making the Actin Reconcentration Model difficult to test experimentally. However, the predictions of the model depend on two properties of the more accessible cell membrane: its ability to transport water and ions. The membrane's hydraulic permeability can be reduced by inhibiting membrane water channels with mercurial sulfhydryl reagents (Agre et al., 1993). However, this would inhibit water influx during the initial swelling as well as water efflux following the movement of salt out of the process. Alternatively, inhibiting the ion pumps (e.g., by ouabain (Stein, 1990)) would prevent salt from being removed from the system and prevent the reconcentration of actin in the reservoir. The extension rate would then drop dramatically, falling to diffusion-only levels (i.e., from curve g′ to curve f′ in Fig. 5, *a* and *b*). No other models for acrosomal process extension rely on ion pumps, so any decrease in extension speed seen when those pumps are inhibited would be evidence in favor of the Actin Reconcentration Model.

Extension to other systems

In principle, the Actin Reconcentration Model could be applied to the extension of the acrosomal processes of other echinoderms. For many such species, the acrosomal reaction is similar to that of *Thyone* (Dan, 1967), although the lengths of the final processes are usually much shorter. However, the data necessary to set system parameters may be more difficult to find, as the acrosomal process of *Thyone* seems to have been studied in more detail than that of other organisms.

Other systems with actin-based motility such as goldfish keratocytes and *Listeria monocytogenes* do not have the difficulty that *Thyone* does with actin delivery. In those systems, actin monomers are stored relatively close to the sites where polymerization takes place, so diffusion is fast enough to supply monomers. In addition, none of those systems exhibits rapid ion and water movement, so the Actin Reconcentration Model is probably not relevant.

CONCLUSIONS

Previous theoretical studies of the extension of *Thyone*'s acrosomal process have concluded that diffusion cannot deliver actin to the tip fast enough to support the observed extension speeds. These models also overlooked some important features of the system. The results of our Actin Reconcentration Model suggest that, due to the effects of nonideality and the concentrating effects of ion and water export, diffusion is much faster than previously thought. The model quantitatively predicts extension speeds in the range of those observed experimentally using values from the literature for all parameters. Both salt transport and solution nonideality are ubiquitous and well-understood phenomena. It appears that their concerted action in the acrosomal process of *Thyone* creates exceptional functional behavior.

APPENDIX

Details of the numerical model

This appendix contains the details of the numerical solution described in the fourth section. The acrosomal process is divided into cylindrical segments of length ℓ and radius r. The segments are indexed by m, with $m = 0$ adjacent to the periacrosomal reservoir and $m = m_{tip}$ at the tip. The periacrosomal compartment is labeled as if it were another cylindrical segment with $m = res$. Because the overall length L of the process is rarely an even multiple of ℓ, segment m_{tip} is of variable length: $\ell_{tip} = L - m_{tip}\ell$. The full cross-sectional area of the cylindrical process is πr^2, but the cross-sectional area accessible for diffusion (unoccupied by filaments) is $A_d < \pi r^2$. The fluid filled volume of segment m is then $V_m = A_d\ell$ for $0 \leq m < m_{tip}$. For $m = m_{tip}$, $V_{m_{tip}} = A_d\ell_{tip}$. The surface area of a segment is $S_m = 2\pi r\ell$ for $0 \leq m < m_{tip}$, and $S_{m_{tip}} = 2\pi r\ell_{tip} + \pi r^2$ for $m = m_{tip}$. Because the surface area of the entire system is fixed at S_0, the surface area

of the reservoir is the area of the membrane not in the process: $S_{res} = S_0 - \pi r^2 - 2\pi rL$.

The concentration of each solute is tracked in each segment as a function of time. The solutes are denoted by the subscript $i = a$, α, or β, corresponding to actin and the two types of salts, respectively. $c_{i,m}$ is the concentration and $a_{i,m}$ is the activity of the ith solute in the mth segment. By integrating Eq. 23 over a time step Δt and segment length ℓ, we arrive at the discrete diffusion-convection equation for segments $0 < m < m_{tip} - 1$:

$$c_{i,m}(t + \Delta t) = c_{i,m}(t) + \left[D_i \frac{a_{i,m+1} - 2a_{i,m} + a_{i,m-1}}{\ell} A_d \Delta t + c_{i,m-1} \Delta V^f_{m-1\to m} - c_{i,m} \Delta V^f_{m\to m+1} + \lambda_{i,m} \right] \frac{1}{V_m} \quad \text{(A1)}$$

where D_i is the diffusion coefficient of the ith solute, and $\lambda_{i,m}$ is the number of particles of the ith species that leave the solution from segment m during a time step Δt (from the Λ_i in Eq. 23). The fluid speed v in Eq. 23 has been rewritten in terms of the volume of fluid $\Delta V^f_{m\to m+1}$ that moves from segment m to segment $m + 1$ in a time step Δt.

The volume of fluid that is drawn from segment m into segment $m + 1$, $\Delta V^f_{m\to m+1}$, includes the volume needed to fill the extending process and the sum of all the volume leaving segments further forward than segment m. The volume needed to fill the process is a function of the extension speed: $v_{ext} A_d \Delta t$. The volume of fluid that moves through the membrane depends on the osmotic pressure difference across the membrane. Expressed as a concentration difference, the osmotic driving force in segment m is (see Eq. 26)

$$\Delta\Pi_m = \Pi_{ext} - c_{\alpha,m} - c_{\beta,m}, \quad \text{(A2)}$$

where Π_{ext} is the external osmotic pressure. Equations 25 and A2 together imply that the volume of water ΔV^{Π}_m that will cross the membrane area S_m in a time Δt under a driving force $\Delta\Pi_m$ is

$$\Delta V^{\Pi}_m = \nu_w P_w S_m \Delta t \Delta\Pi_m, \quad \text{(A3)}$$

where P_w is the hydraulic permeability of the membrane, and ν_w is the volume of a water molecule (to convert from the particle flux given by the other terms in the equation to a volume flux). The total fluid volume that leaves segment m is therefore

$$\Delta V^f_{m\to m+1} = v_{ext} A_d \Delta t + \sum_{n=m+1}^{m_{tip}} \Delta V^{\Pi}_n. \quad \text{(A4)}$$

The sink terms $\lambda_{i,m}$ are straightforward. The α-salt ions experience no net transport in or out of the system, so $\lambda_{\alpha,m} = 0$ everywhere. Actin is only polymerized at the tip, so $\lambda_{a,m} = 0$ for $m \neq m_{tip}$. For $m = m_{tip}$,

$$\lambda_{a,m_{tip}} = -(N_f/\delta) v_{ext} \Delta t, \quad \text{(A5)}$$

where N_f is the total number of actin filaments in the process, and v_{ext} is the extension speed of the process. For the β-salt there is net transport. Using Eq. 13,

$$\lambda_{\beta,m} = -j_{\beta\text{-max}} \frac{c_{\beta,m}}{c_{\beta,m} + c_{\beta,1/2}} S_m \Delta t, \quad \text{(A6)}$$

where the sign explicitly indicates a movement of particles out of the process. A similar equation for the β-salt ions applies in the reservoir.

The iteration begins just after the beginning of the acrosomal reaction. The initial influx of ions and the swelling of the periacrosomal region are not modeled in detail. Instead, the initial volume of the reservoir is set to the doubled value ($V_{res}(0) = 2V_0$), and the initial concentrations of actin and the ions are set to their post-swelling values: $c_{i,res}(0) = N_{i0}/(2V_0)(i = a, \alpha, \text{or } \beta)$. The initial length of the process L_0 is chosen so that there are initially two segments, and the concentration of actin in these segments is initially the same as in the reservoir.

Once each time step, the solute concentrations in the process and reservoir are updated using Eq. A1. Each update begins with actin polymerization at the process tip. The extension speed can be calculated from the polymerization rate. Then the new concentrations are calculated, beginning in the tip segment. The solute concentrations in the tip segment change not only due to diffusion and bulk fluid flow, but also due to polymerization. Furthermore, extension of the process changes the size of the tip segment. After the tip segment is updated completely, the concentrations in each segment in the rest of the process are updated, working front to back. Finally, the concentrations in the reservoir are updated. The details of these steps are described in the remainder of this section.

The extension speed v_{ext} is given by the Brownian Ratchet Model (Eq. 24). The relevant activity a_a is in principle the activity of actin at the tip, $a_{a,m_{tip}}$. However, the length of segment m_{tip} is ~0.1 μm: probably larger than the region in which polymerization takes place. So in order to better represent the actin concentration profile near the tip without using a drastically smaller segment size, the concentration of actin is extrapolated to the forward end of segment m_{tip}:

$$c_{a,end} = \frac{\ell + 2\ell_{tip}}{\ell + \ell_{tip}} c_{a,m_{tip}} - \frac{\ell_{tip}}{\ell + \ell_{tip}} c_{a,m_{tip}-1}. \quad \text{(A7)}$$

The extension speed is then found by using Eq. 24 (calculating the activity from the concentration in Eq. A7 via Eq. 18). The new process length is then:

$$L(t + \Delta t) = L(t) + v_{ext} \Delta t. \quad \text{(A8)}$$

The solute concentrations in segment m_{tip} are then updated using the relevant variation of Eq. A1:

$$c_{i,m_{tip}}(t + \Delta t) = c_{i,m_{tip}}(t) + \left[D_i \frac{a_{i,m_{tip}-1} - a_{i,m_{tip}}}{\ell_{tip}/2 + \ell/2} A_d \Delta t + c_{i,m_{tip}-1} \Delta V^f_{m_{tip}-1\to m_{tip}} + \lambda_{i,m_{tip}} \right] \frac{1}{V_{m_{tip}}}. \quad \text{(A9)}$$

In Eq. A9, the denominator of the diffusion term has been adjusted to account for the nonstandard length of segment m_{tip}.

Because the right-hand side of Eq. A9 is evaluated at time step t, the new tip concentrations at time $t + \Delta t$ have been calculated for the volume of the old tip segment. The process, however, has grown, and therefore the length of segment m_{tip} must be updated to reflect the new overall length of the process. It becomes $\ell'_{tip} = \ell_{tip} + v_{ext}\Delta t$, and the concentrations of the solutes in segment m_{tip} are adjusted so that matter is conserved:

$$c'_{i,m_{tip}} = c_{i,m_{tip}} \frac{V_{m_{tip}}}{A_d \ell'_{tip}}. \quad \text{(A10)}$$

Clearly segment m_{tip} cannot grow indefinitely. Although it is most natural to allow it to grow until it reaches length ℓ and then to add another segment (labeled $m_{tip} + 1$), the procedure has a practical drawback. If the process were to extend only a small distance into the newly added segment, the volume of that segment would be much smaller than the typical segment, and the calculation could become unstable. To avoid that situation, segment m_{tip} is allow to vary in length in the range $\ell < \ell_{tip} < 3\ell/2$ rather than $0 < \ell_{tip} < \ell$. When the segment becomes longer than $3\ell/2$, it is split into two segments, one of length ℓ and one of the remaining length, $L - (m_{tip} + 1)\ell > \ell/2$. In this way, the segment does not become very small, and the calculation remains stable. The concentrations in the two segments after the split must again be adjusted. They are set so that all solutes are conserved, and so the extrapolated actin concentration of Eq.

A7 does not change:

$$c'_{a,m_{tip}+1} = \frac{\ell'_{tip} + 2\ell}{\ell'_{tip} + \ell} c_{a,m_{tip}} - \frac{\ell}{\ell'_{tip} + \ell} c_{a,m_{tip}-1}$$
$$c'_{a,m_{tip}} = (c_{a,m_{tip}} \ell A_d - c'_{a,m_{tip}+1} V_{m_{tip}+1}) \frac{1}{A_d \ell}, \quad \text{(A11)}$$

where the primed concentrations are those after segment m_{tip} is split into segments m_{tip} and $m_{tip} + 1$.

After the update step in segment m_{tip}, segments $m = m_{tip} - 1$ to $m = 0$ are updated using Eq. A1, looping backward from the tip to the reservoir. Then the reservoir is updated. Because the reservoir becomes depleted of solutes and fluid volume, the absolute number of solute molecules and the volume of the reservoir are calculated instead of the solute concentrations. The reservoir loses all of the volume that has moved into the process and through the process membrane as well as volume through its own membrane:

$$V_{res}(t + \Delta t) = V_{res}(t) - \Delta V^{f}_{res \to 0} - \Delta V^{\Pi}_{res}. \quad \text{(A12)}$$

Because the reservoir has only one neighboring segment, the update equation is

$$N_{i,res}(t + \Delta t) = N_{i,res}(t) + \left[D_i \frac{a_{i,0} - a_{i,res}}{\ell} - c_{i,res} \Delta V^{f}_{res \to 0} \right] A_d \Delta t + \lambda_{i,res}, \quad \text{(A13)}$$

where $N_{i,res}$ is the number of molecules of the appropriate solute in the reservoir. The solute concentrations in the reservoir are then simply

$$c_{i,res}(t + \Delta t) = \frac{N_{i,res}(t + \Delta t)}{V_{res}(t + \Delta t)}. \quad \text{(A14)}$$

This work was supported by the National Science Foundation under Grant HRD-9021929 and the National Institutes of Health under Grant HL-36546.

REFERENCES

Agre, P., G. M. Preston, B. L. Smith, J. S. Jung, S. Raina, C. Moon, W. B. Guggino, and S. Nielsen. 1993. Aquaporin CHIP: the archetypal molecular water channel. *Am. J. Physiol.* 265:F463–F476.

Arfken, G. 1985. Mathematical Methods for Physicists. Academic Press, New York.

Bray, D., and J. G. White. 1988. Cortical flow in animal cells. *Science.* 239:885–888.

Cantor, C. R., and P. R. Schimmel. 1980. Biophysical Chemistry II: Techniques for the Study of Biological Structure and Function. W. H. Freeman and Company, San Francisco.

Colwin, L. H., and A. L. Colwin. 1955. The spermatozoon and sperm entry in the egg of the holothurian, *Thyone briareus. Biol. Bull.* 109:357–358.

Condeelis, J. 1993. Life at the leading edge: the formation of cell protrusions. *Annu. Rev. Cell Biol.* 9:411–444.

Conrad, P. A., M. A. Nederlof, I. M. Herman, and D. L. Taylor. 1989. Correlated distribution of actin, myosin, and microtubules at the leading edge of migrating Swiss 3T3 fibroblasts. *Cell Motil. Cytoskeleton.* 14:527–543.

Cooper, J. A. 1991. The role of actin polymerization in cell motility. *Annu. Rev. Physiol.* 53:585–605.

Cossart, P. 1995. Actin-based bacterial motility. *Curr. Opin. Cell Biol.* 7:94–101.

Cudmore, S., P. Cossart, G. Griffiths, and M. Way. 1995. Actin-based motility of vaccinia virus. *Nature.* 378:636–638.

Dan, J. C. 1967. Acrosome reaction and lysins. *In* Fertilization. Academic Press, New York. 237–293.

DeBiasio, R. L., L.-L. Wang, G. W. Fisher, and D. L. Taylor. 1988. The dynamic distribution of fluorescent analogues of actin and myosin in protrusions at the leading edge of migrating Swiss 3T3 fibroblasts. *J. Cell Biol.* 107:2631–2645.

DeRosier, D. J., and L. G. Tilney. 1984. The form and function of actin. *In* Cell and Muscle Motility. Plenum Press, New York. 139–169.

Goldberg, M. B., and J. A. Theriot. 1995. *Shigella flexneri* surface protein IcsA is sufficient to direct actin-based motility. *Proc. Natl. Acad. Sci. USA.* 92:6572–6576.

Grebecki, A. 1994. Membrane and cytoskeleton flow in motile cells with emphasis on the contribution of free-living amoebae. *Int. Rev. Cytol.* 148:37–80.

Gros, G. 1978. Concentration dependence of the self-diffusion of human and *Lumbricus terrestris* hemoglobin. *Biophys. J.* 22:453–468.

Han, J., and J. Herzfeld. 1993. Macromolecular diffusion in crowded solutions. *Biophys. J.* 65:1155–1161.

Han, J., and J. Herzfeld. 1994. The freezing transition of bidisperse hard spheres: a simple model. *Mol. Phys.* 82:617–628.

Heinzen, R. A., S. F. Hayes, M. G. Peacock, and T. Hackstadt. 1993. Directional actin polymerization associated with spotted fever group Rickettsia infection of vero cells. *Infect. Immun.* 61:1926–1935.

Hermans, J. J. 1947. Diffusion with discontinuous boundary. *J. Colloid Sci.* 2:387–398.

Inoué, S., and L. G. Tilney. 1982. Acrosomal reaction of *Thyone* sperm I. Changes in the sperm head visualized by high resolution video microscopy. *J. Cell Biol.* 93:812–819.

Katchalsky, A., and P. F. Curran. 1967. Nonequilibrium Thermodynamics in Biophysics. Harvard University Press, Cambridge.

Lanni, F., D. L. Taylor, and B. R. Ware. 1981. Fluorescence photobleaching recovery in solutions of labeled actin. *Biophys. J.* 35:351–364.

Lanni, F., and B. R. Ware. 1984. Detection and characterization of actin monomers, oligomers, and filaments in solution by measurement of fluorescence photobleaching recovery. *Biophys. J.* 46:97–110.

Lee, J., A. Ishihara, J. A. Theriot, and K. Jacobson. 1993. Principles of locomotion for simple-shaped cells. *Nature.* 362:167–171.

Lide, D. R. 1998. CRC Handbook of Chemistry and Physics. CRC Press, Boca Raton.

Macey, R. I., and J. Brahm. 1989. Osmotic and diffusional water permeability in red cells: methods and interpretations. *In* Water Transport in Biological Membranes. CRC Press, Boca Raton. 26–39.

Mitchison, T. J., and L. P. Cramer. 1996. Actin-based cell motility and cell locomotion. *Cell.* 84:371–379.

Muramatsu, N., and A. P. Minton. 1988. Tracer diffusion of globular proteins in concentrated protein solutions. *Proc. Natl. Acad. Sci. USA.* 85:2984–2988.

Olbris, D. J., and J. Herzfeld. 1996. Variation of the rate of extension of actin networks. *In* Materials Research Society. Materials Research Society, Boston. 129–134.

Oster, G. F., and A. S. Perelson. 1987. The physics of cell motility. *J. Cell Sci.* (Suppl.)8:35–54.

Oster, G. F., A. S. Perelson, and L. G. Tilney. 1982. A mechanical model for elongation of the acrosomal process in Thyone sperm. *J. Math Biol.* 15:259–265.

Pantaloni, D., and M.-F. Carlier. 1993. How profilin promotes actin filament assembly in the presence of thymosin β4. *Cell.* 75:1007–1014.

Perelson, A. S., and E. A. Coutsias. 1986. A moving boundary model of acrosomal elongation. *J. Math Biol.* 23:361–379.

Peskin, C. S., G. M. Odell, and G. F. Oster. 1993. Cellular motions and thermal fluctuations: the Brownian Ratchet. *Biophys. J.* 65:316–324.

Pollard, T. D. 1986. Rate constants for the reactions of ATP- and ADP-actin with the ends of actin filaments. *J. Cell Biol.* 103:2747–2754.

Pring, M., A. Weber, and M. R. Bubb. 1992. Profilin-actin complexes directly elongate actin filaments at the barbed end. *Biochemistry.* 31: 1827–1836.

Sanger, J. M., R. Chang, F. Ashton, J. B. Kaper, and J. W. Sanger. 1996. Novel form of actin-based motility transports bacteria on the surface of infected cells. *Cell Motil. Cytoskeleton.* 34:279–287.

Schackmann, R. W., R. Christen, and B. M. Shapiro. 1981. Membrane potential depolarization and increased intracellular pH accompany the acrosome reaction of sea urchin sperm. *Proc. Natl. Acad. Sci. USA.* 78:6066–6070.

Sejersted, O. M. 1988. Maintenance of Na, K-homeostasis by Na, K-pumps in striated muscle. *In* The Na+, K+-Pump, Part B: Cellular Aspects. Alan R. Liss, New York.

Smith, S. J. 1988. Neuronal cytomechanics: the actin-based motility of growth cones. *Science.* 242:708–715.

Southwick, F. S., and D. L. Purich. 1994. Dynamic remodeling of the actin cytoskeleton: lessons learned from *Listeria* locomotion. *BioEssays.* 16: 885–891.

Stein, W. D. 1990. Channels, Carriers, and Pumps: An Introduction to Membrane Transport. Academic Press, San Diego.

Tait, J. F., and C. Frieden. 1982. Polymerization and gelation of actin studied by fluorescence photobleaching recovery. *Biochemistry.* 21: 3666–3674.

Teysseire, N., C. Chiche-Portiche, and D. Raoult. 1992. Intracellular movements of *Rickettsia conorii* and *R. typhi* based on actin polymerization. *Res. Microbiol.* 143:821–829.

Theriot, J. A. 1995. The cell biology of infection by intracellular bacterial pathogens. *Annu. Rev. Cell Dev. Biol.* 11:213–239.

Theriot, J. A., and T. J. Mitchison. 1991. Actin microfilament dynamics in locomoting cells. *Nature.* 352:126–131.

Theriot, J. A., and T. J. Mitchison. 1992. Comparison of actin and cell surface dynamics in motile fibroblasts. *J. Cell Biol.* 119:367–377.

Theriot, J. A., and T. J. Mitchison. 1993. The three faces of profilin. *Cell.* 75:835–838.

Theriot, J. A., T. J. Mitchison, L. G. Tilney, and D. A. Portnoy. 1992. The rate of actin-based motility of intracellular *Listeria monocytogenes* equals the rate of actin polymerization. *Nature.* 357:257–260.

Tilney, L. G. 1978. The polymerization of actin V. A new organelle, the actomere, that initiates the assembly of actin filaments in *Thyone* sperm. *J. Cell Biol.* 77:551–564.

Tilney, L. G. 1979. Actin, motility, and membranes. *In* Membrane Transduction Mechanisms. Raven Press, New York. 163–186.

Tilney, L. G., D. J. DeRosier, and M. S. Tilney. 1992a. How *Listeria* exploits host cell actin to form its own cytoskeleton. I. Formation of a tail and how that tail might be involved in movement. *J. Cell Biol.* 118:71–81.

Tilney, L. G., D. J. DeRosier, A. Weber, and M. S. Tilney. 1992b. How *Listeria* exploits host cell actin to form its own cytoskeleton. II. Nucleation, actin filament polarity, filament assembly, and evidence for a pointed end capper. *J. Cell Biol.* 118:83–93.

Tilney, L. G., and S. Inoué. 1982. Acrosomal reaction of *Thyone* sperm. II. The kinetics and possible mechanism of acrosomal process elongation. *J. Cell Biol.* 93:820–827.

Tilney, L. G., and S. Inoué. 1985. Acrosomal reaction of *Thyone* sperm III. The relationship between actin assembly and water influx during the extension of the acrosomal process. *J. Cell Biol.* 100:1273–1283.

Tilney, L. G., and N. Kallenbach. 1979. Polymerization of actin VI. The polarity of the actin filaments in the acrosomal process and how it might be determined. *J. Cell Biol.* 81:608–623.

Tilney, L. G., D. P. Kiehart, C. Sardet, and M. Tilney. 1978. The polymerization of actin IV. Role of Ca^{++} and H^{+} in the assembly of actin and in membrane fusion in the acrosomal reaction of echinoderm sperm. *J. Cell Biol.* 77:536–550.

Wolfram, S. 1996. The Mathematica Book. Wolfram Media/Cambridge University Press, New York.

Zhu, C., and R. Skalek. 1988. A continuum model of protrusion of pseudopod in leukocytes. *Biophys. J.* 54:1115–1137.